Supporting Information

Acoustic Vibrations of Al Nanocrystals: Size, Shape, and Crystallinity Revealed by Single-Particle Transient Extinction Spectroscopy

Behnaz Ostovar[†∥], Man-Nung Su[‡∥¶], David Renard[‡∥], Benjamin D. Clark[‡∥], Pratiksha D. Dongare[§∥], Chayan Dutta[‡∥], Niklas Gross[‡∥], John E. Sader[○], Christy F. Landes[†‡⊥∥#], Wei-Shun Chang[▽], Naomi J. Halas[†‡Δ∥#], and Stephan Link[†‡∥#]*

[†]Department of Electrical and Computer Engineering, [‡]Department of Chemistry, [§]Applied Physics Graduate Program, [Δ]Department of Physics and Astronomy, [⊥]Department of Chemical and Biomolecular Engineering, [∥]Laboratory for Nanophotonics, and [#]Smalley-Curl Institute, Rice University, 6100 Main Street, Houston, Texas 77005, USA

[○]ARC Centre of Excellence in Exciton Science, School of Mathematics and Statistics, The University of Melbourne, Parkville, VIC 3010, Australia

[▽]Department of Chemistry and Biochemistry, University of Massachusetts Dartmouth, 285 Old Westport Rd., North Dartmouth, Massachusetts 02747, USA

[*]Corresponding author email: slink@rice.edu

[¶]Present address: Department of Chemistry, University of California, Berkeley, California 94720, USA.

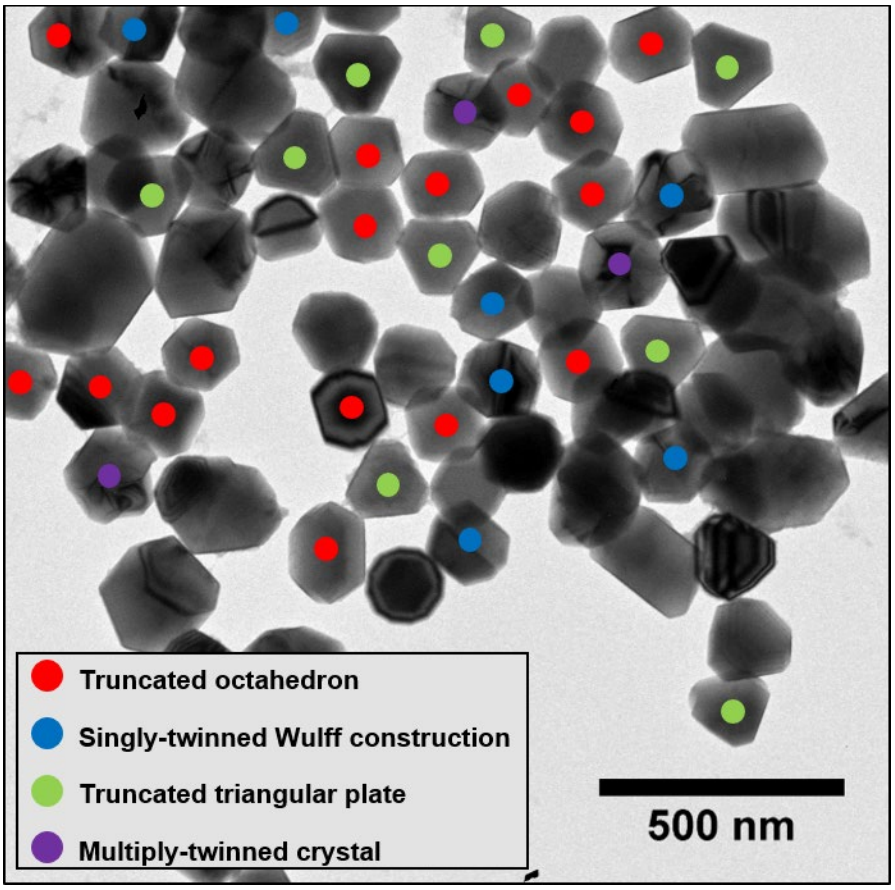

Figure S1. Transmission electron microscopy (TEM) image of aluminum nanocrystals (AlNCs) showing the different shapes observed within one sample of colloidal nanoparticles: truncated octahedron, singly-twinned Wulff construction, truncated triangular plate, and multiply-twinned crystal.

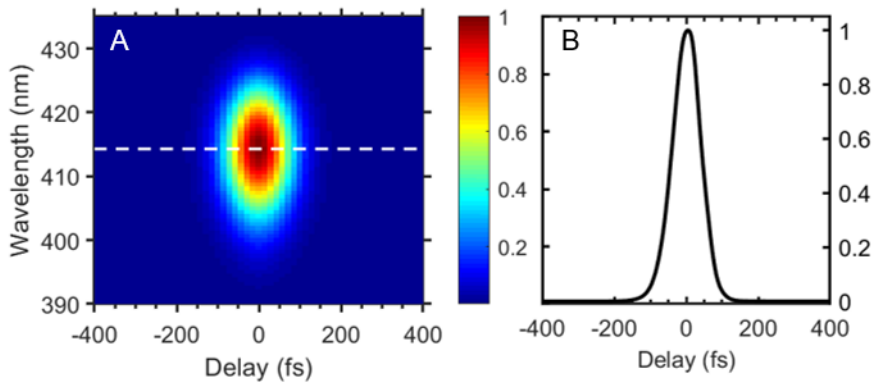

Figure S2. Characterization of the fundamental laser pulses provided by the Ti-Sapphire laser and used to generate the pump and probe pulses in the transient extinction microscope. Frequency resolved optical gating (FROG) was used for the pulse characterization employing a Swamp Optics GRENOUILLE. The FROG image is shown in (A) and the white dashed line indicates a horizontal slice corresponding to the pulse temporal autocorrelation intensity given in (B). From the pulse intensity versus time a pulse duration of 95 fs was determined at a center wavelength of 828 nm.

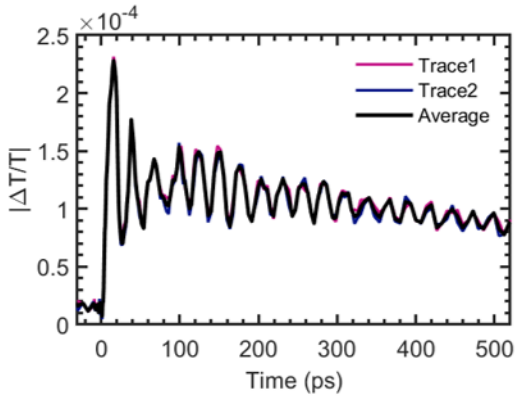

Figure S3. No structural damage of the nanoparticles due to laser heating was observed as illustrated here by repeatedly recording transient transmissions of the same single colloidal AlNC with a diameter of 132 nm. The fundamental laser wavelength was used for excitation and a probe wavelength of 650 nm was chosen. The pump and probe power densities were 8.56×10^4 W/cm^2 and 1.41×10^4 W/cm^2, respectively.

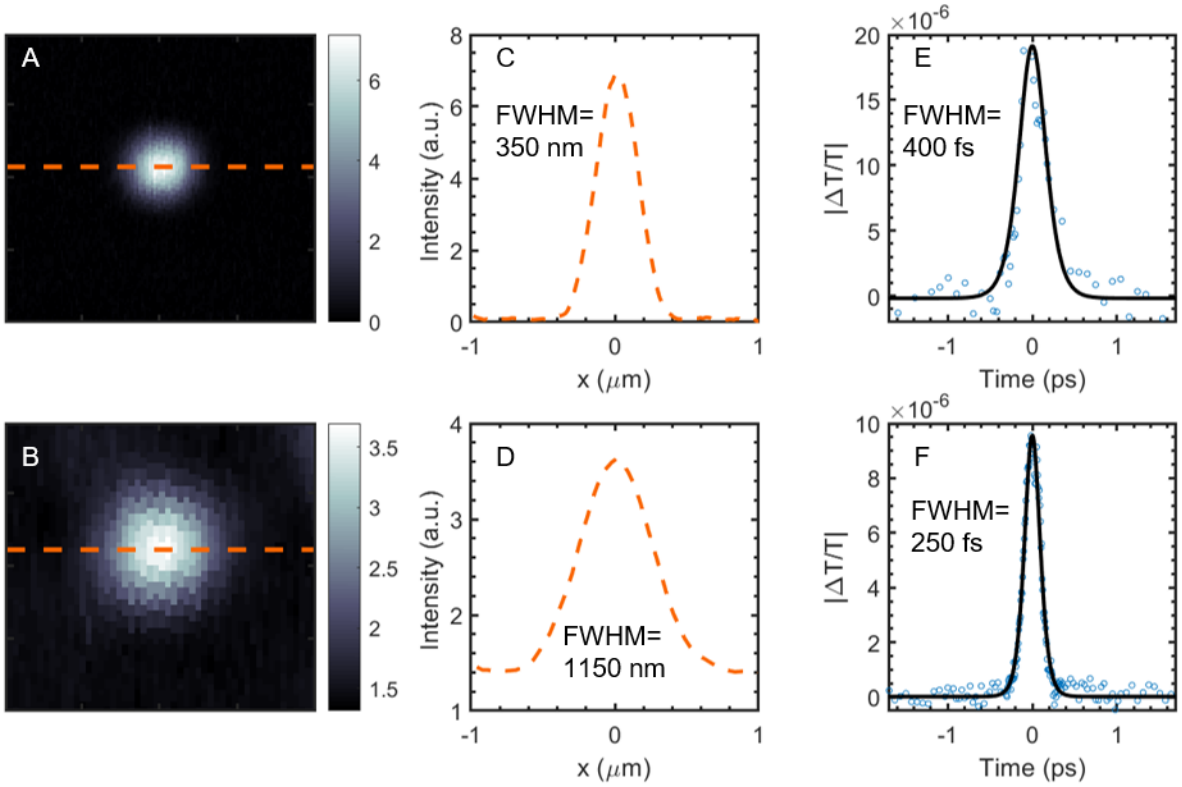

Figure S4. Transient extinction images of single gold nanodisks with a diameter of 160 nm and a height of 35 nm recorded by temporally and spatially overlapping the excitation pulse at the fundamental laser wavelength with the probe pulse at 700 nm using (A) a refractive objective (Zeiss Plan-Apochromat, 63X and numerical aperture (N.A.) of 1.4) and (B) a reflective objective (Ealing, 36X, N.A. = 0.5). The pump power densities were 8.56×10^4 W/cm^2 and 7.90×10^3 W/cm^2, respectively and the probe power densities were 1.41×10^4 W/cm^2 and 4.84×10^2 W/cm^2, respectively. Orange dashed lines indicate the spatial line sections given in (C) and (D). The full width at half maximum (fwhm) of the line sections yields the spatial resolution of our setup under these conditions. Corresponding temporal instrument response functions (IRFs) using (E) the refractive objective and (F) the reflective objective were determined by cross-correlation of pump and probe beams. The black lines show a fit to a Sech^{2}x function. Using a reflective objective improves the time resolution at the expense of spatial resolution.

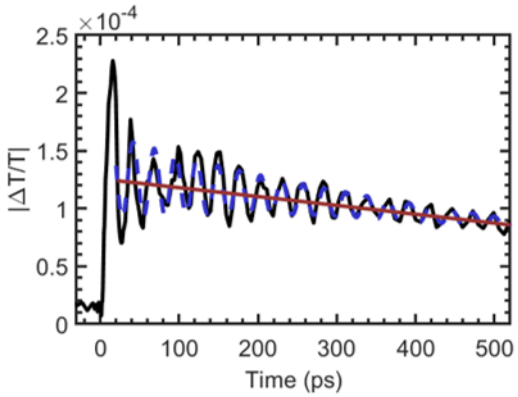

Figure S5. Analysis of the experimental acoustic vibrations. As an example shown here is the transient transmission of a single colloidal AlNC with a diameter of 132 nm. The fundamental laser wavelength was used for excitation and a probe wavelength of 650 nm was chosen. The pump and probe power densities were 8.56×10^4 W/cm^2 and 1.41×10^4 W/cm^2, respectively. Neglecting early delay times (< 15 ps), the dashed blue line shows a fit using the following equation:

$$\frac{\Delta T}{T} = A_1 \exp\left(-\frac{t}{\tau_1}\right) + A_{HO} \exp\left(-\frac{t}{\tau_{HO}}\right) \cos(2\pi t\nu - \phi) \qquad \text{(S1)}$$

Here A_1 and τ_1 are the amplitude and decay time of the exponential decay corresponding to phonon-phonon relaxation (see red line in Figure S5), while the acoustic vibration is described by A_{HO} as the amplitude, ν as the frequency, τ_{HO} as the damping time, and ϕ as a phase factor. To isolate only the acoustic vibration part as done in the figures of the main text, the first term in Equation S1 was subtracted from the data. The starting value for ν in the fitting procedure was taken from a fast Fourier transform (FFT) analysis.

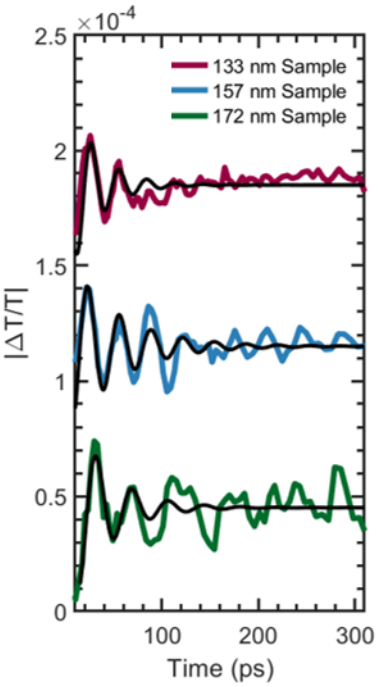

Figure S6. Averaging transient transmissions of all AlNCs within one sample results in a reduced vibration amplitude and shorter damping time. Transient transmissions were added together and averaged for all 19 AlNCs from the 133 ± 15 nm sample (red), all 21 AlNCs from the 157 ± 19 nm sample (blue), and all 9 AlNCs from the 172 ± 23 nm sample (green). Data are offset for better comparison. The fundamental laser wavelength was used for excitation and a probe wavelength of 650 nm was chosen close to the LSPR maximum. The pump and probe power densities were 8.56×10^4 W/cm^2 and 1.41×10^4 W/cm^2, respectively. The black line indicates a fit to the data using a damped cosine function (Equation 2), yielding vibration frequencies of 38.2GHz, 28.9 GHz, and 26.7 GHz for three samples. The damping times are 29.1 ps, 51.1 ps, and 37.3 ps, respectively. While the average vibration frequencies agree reasonably well with the single-particle measurements, the damping times are significantly shorter. The fits are also poorer for the data shown in Figure S6.

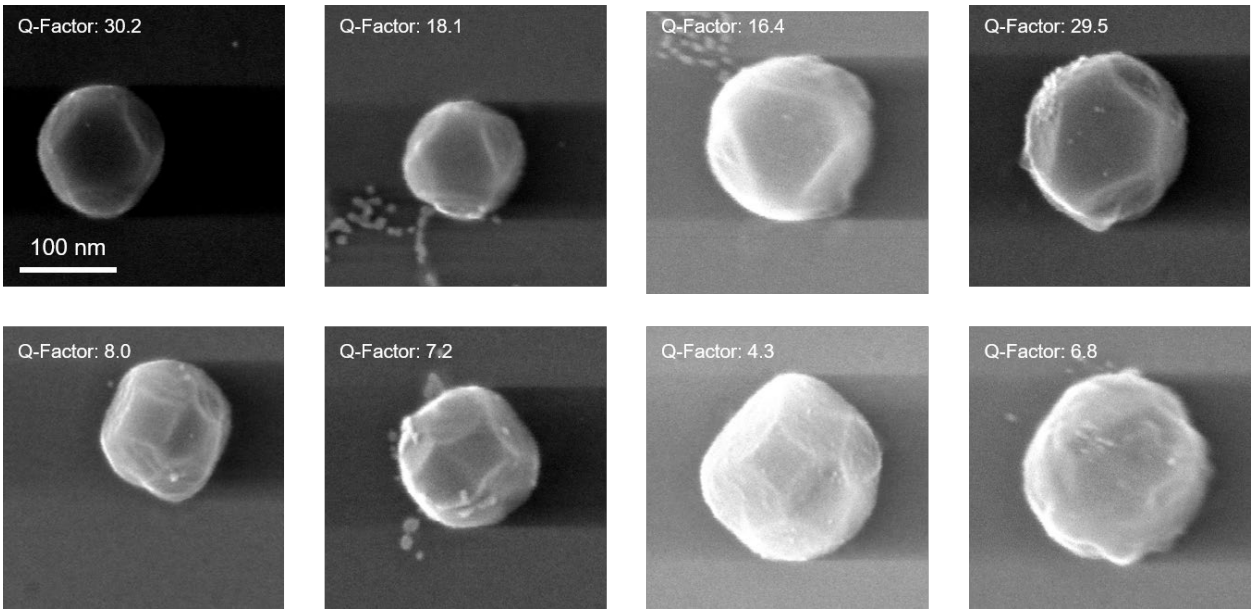

Figure S7. Scanning electron microscopy (SEM) images of the quasi-spherical AlNCs possessing high Q-factors (top row) and low Q-factors (bottom row). The AlNCs in the top row, all having high Q-factors, are truncated octahedra, known to be single-crystalline. The AlNCs in the bottom row with low Q-factors have the shapes of a singly-twinned Wulff construction or a Marks decahedron, which have one or five twin planes, respectively. Differences in the degree of crystallinity therefore explain the variation in observed Q-factors.

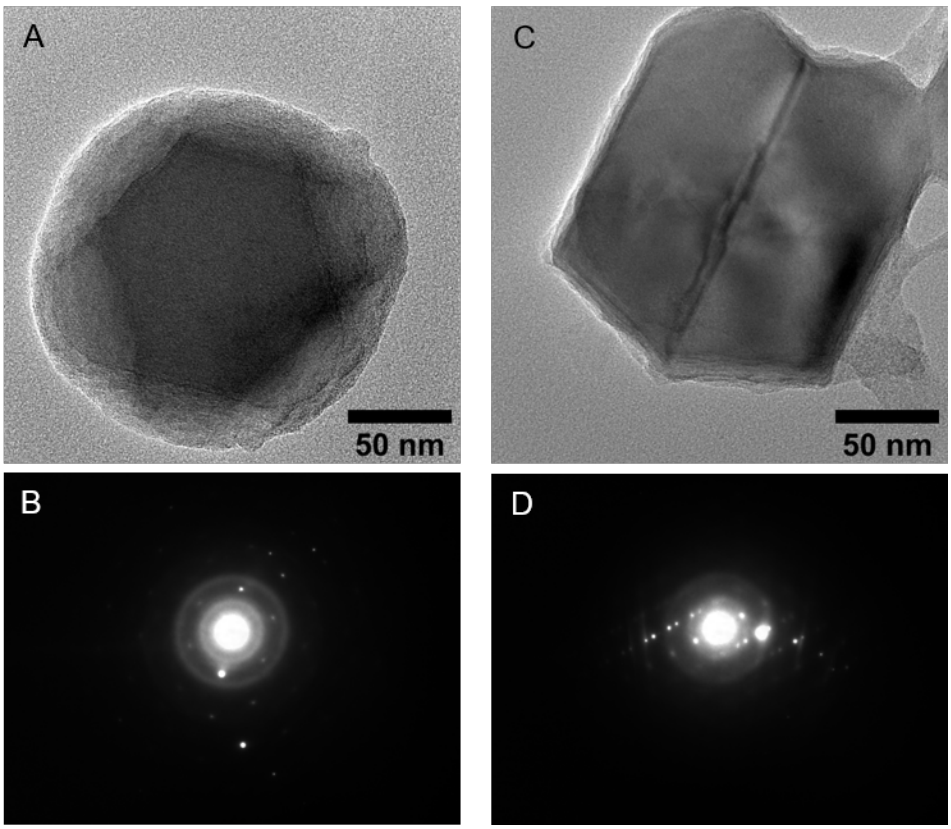

Figure S8. (A)TEM image and (B) electron diffraction pattern of a truncated octahedron AlNC showing a characteristic diffraction from a face-centered cubic (FCC) metal crystal with no twin defects. The electron diffraction reveals a hexagonal pattern composed of only one diffracted spot at each location. (C)TEM image and (D) electron diffraction pattern of a twinned Wulff construction AlNC showing characteristic diffraction from a FCC metal crystal with one twin defect. The electron diffraction pattern shows a doubling of every diffracted spot, indicative of two crystal orientations.

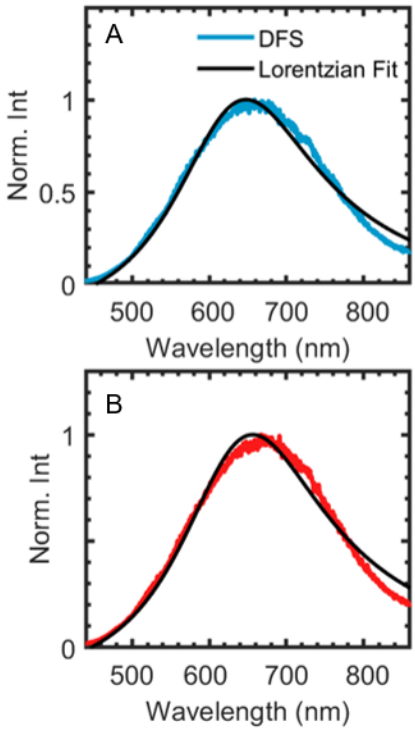

Figure S9. Correlated single-particle scattering spectra of AlNCs shown in Figure 3B of the main text with different crystallinity. Scattering spectra of a AlNC with a diameter of 161 nm (A) and 167 nm (B). Lorentzian fits to the scattering spectra are shown as black lines. The scattering maxima and linewidths obtained from the fits are 647 nm and 298 nm (A) and 656 nm and 306 nm (B). The difference between these two spectra is small compared to their vibrational quality factors (Q-factors). For these larger AlNCs, the plasmon itself appears to only weakly depend on nanoparticle crystallinity. Scattering spectra were acquired using a 50X air objective with a N.A. of 0.8 (Zeiss EC Epiplan-Neofluar) on a home-built dark-field scattering microscope described in [1]

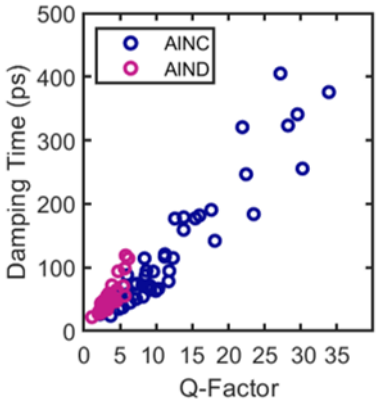

Figure S10. Damping times versus Q-factors for 49 quasi-spherical colloidal AlNCs (dark blue) and 41 lithographically fabricated AlNDs (pink). The particles were pumped at the fundamental laser wavelength (power densities of 9.40×10^4 W/cm^2 and 7.52×10^4 W/ cm^2, respectively) and probed at 650 nm (power densities of 1.41×10^4 W/cm^2 and 1.41×10^4 W/ cm^2, respectively). Diameters of AlNCs ranged from 110 nm to 250 nm and AlNDs had dimensions ranging from 170 nm to 350 nm. The raw data used for the analysis of the lithographically fabricated AlNDs was taken from [2].

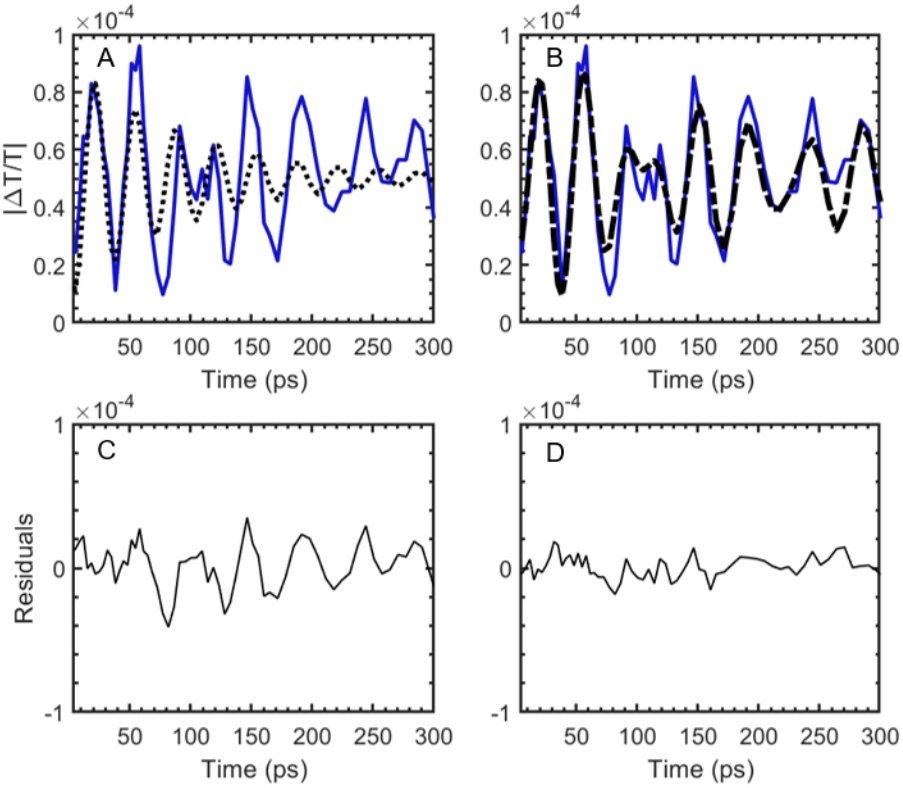

Figure S11. Comparison of fits to the acoustic vibrations of a triangular-shaped AlNC with an edge length of 160 nm when using (A) one damped harmonic oscillation according to Equation 2 and (B) two damped harmonic oscillations as described by Equation 3. Corresponding residuals are presented in (C) and (D). When using only one damped harmonic oscillation the residuals in (C) clearly indicate a second oscillation. Using two damped harmonic oscillations results in an improved agreement (D). The pump and probe power densities were 8.56×10^4 W/cm^2 and 1.41×10^4 W/cm^2, respectively.

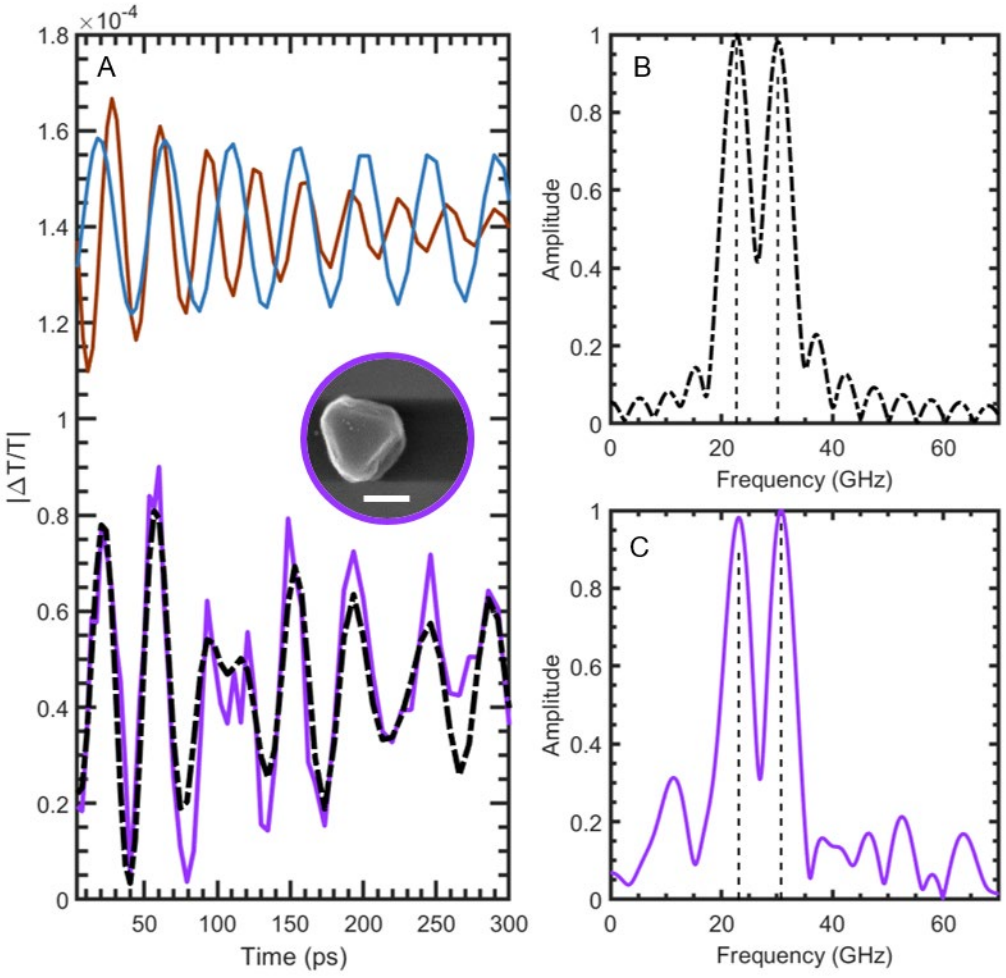

Figure S12. (A) Representative time-dependent transient transmission showing the acoustic vibrations of a triangular-shaped AlNC with an edge length of 160 nm. The dashed black line corresponds to a fit using two cosine terms and exponential decays as described by Equation 3. The two cosine components extracted from the fit are separately shown above the experimental data. The corresponding SEM image of the AlNC is shown in the inset. (B) FFT of the fit to the data (dashed black line in panel (A)), giving vibration frequencies of 30.6 GHz and 22.9 GHz. (C) FFT of the experimental time-dependent transient transmission from panel (A), yielding vibration frequencies of 30.5 GHz and 23.8 GHz. The FFT spectra are normalized to the

intensity of the higher frequency mode. The pump and probe power densities were 8.56×10^4 W/cm^2 and 1.41×10^4 W/cm^2, respectively.

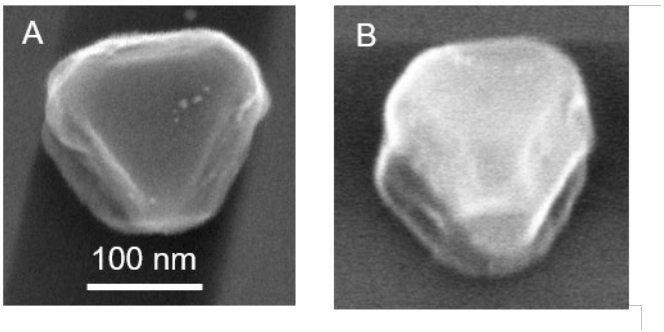

Figure S13. (A) SEM image a representative triangular-shaped AlNC with an edge length of 145 nm. (B) 70° tilted SEM image of the same AlNC. The thickness of this AlNC was determined to be 80-90 nm. Scale bar of 100 nm applies to both images.

REFERENCES

1. Cai, Y.-Y.; Sung, E.; Zhang, R.; Tauzin, L. J.; Liu, J. G.; Ostovar, B.; Zhang, Y.; Chang, W.-S.; Nordlander, P.; Link, S., Anti-Stokes Emission from Hot Carriers in Gold Nanorods. *Nano Lett.* **2019**, *19*, 1067-1073.

2. Su, M.-N., et al., Optomechanics of Single Aluminum Nanodisks. *Nano Lett.* **2017**, *17*, 2575-2583.